agronomy

MDPI

Article

Subsoiling Sustains Winter Wheat Yield with Reduced Nitrogen Input in the North China Plain

Xiaokang Lv, Shitong Zhang, Xuejie Gao, Qin Fang, Hongguang Wang, Dongxiao Li, Jianning He and Ruiqi Li *

State Key Laboratory of North China Crop Improvement and Regulation, Key Laboratory of Crop Growth Regulation of Hebei Province, College of Agronomy, Hebei Agricultural University, Baoding 071000, China; lvxk1993@hebau.edu.cn (X.L.); 20242100254@pgs.hebau.edu.cn (S.Z.); 20247101186@pgs.hebau.edu.cn (X.G.); fangqin@hebau.edu.cn (Q.F.); jlwanghongguang@163.com (H.W.); lidongxiao.xiao@163.com (D.L.); hjn@hebau.edu.cn (J.H.)

* Correspondence: nxylrq@hebau.edu.cn

Abstract

Excessive nitrogen (N) input and repeated shallow tillage constrain sustainable winter wheat production in the North China Plain. A two-year field experiment was conducted to compare rotary tillage, subsoiling, and no-tillage under N application rates of 120, 180, and 240 kg ha^{-1}. Subsoiling generally increased grain yield, with yields under subsoiling at 180 kg N ha^{-1} (SN180) reaching 8129.64 and 7700.89 kg ha^{-1} in the two growing seasons, respectively, without significant differences from SN240, while reducing N input by 60 kg ha^{-1}. SN180 favored post-anthesis dry matter accumulation and post-anthesis N uptake. Accordingly, it achieved partial factor productivity of applied N of 45.16 and 42.78 kg kg^{-1}, and N uptake efficiencies ranging from 1.29 to 1.46 kg kg^{-1}, which were higher than those under SN240 and other tillage practices at the same N rate. In 2023–2024, SN180 increased root length density at 20–40 cm by 41.8% and 59.7% and root dry weight density by 22.0% and 20.5% compared with rotary tillage and no-tillage, respectively. SN180 also maintained relatively high nitrate reductase and glutamine synthetase activities during the same growing season, although the responses varied among plant organs and growth stages. Under the conditions of this two-year field experiment, subsoiling combined with 180 kg N ha^{-1} achieved the most favorable balance between grain yield and N use performance among the treatments tested, indicating its potential as a management option for irrigated winter wheat production in the North China Plain.

Keywords: tillage practice; root morphology; nitrogen use efficiency; post-anthesis nitrogen uptake; nitrogen metabolism

Academic Editor: Witold Grzebisz

Received: 16 July 2026
Revised: 3 September 2026
Accepted: 4 September 2026
Published: 7 September 2026

1. Introduction

Wheat (*Triticum aestivum* L.) is a major crop in the North China Plain of China, one of the country's most important wheat-producing regions, and its stable production is crucial for food security [1,2]. Over the past several decades, sustained productivity gains in this region have been achieved largely through the intensive application of chemical nitrogen (N) fertilizers, coupled with repeated rotary tillage [3,4]. Although this high-input strategy has contributed to significant yield improvements, its environmental and agronomic costs have become increasingly apparent, as evidenced by soil acidification, groundwater nitrate contamination, and elevated greenhouse gas emissions linked to excessive N application [5]. In addition, long-term rotary tillage to a depth of only 10–15 cm has promoted the formation of a dense plow pan beneath the cultivated layer [6]. This

compacted zone restricts root penetration into deeper soil strata, reduces water infiltration, and limits the crop's capacity to access nutrients stored in the subsoil [6,7]. The confluence of these challenges threatens the long-term sustainability of wheat production in the North China Plain and demands integrated management practices that reconcile high yields with improved resource-use efficiency.

Tillage practice and N management are widely recognized as two major agronomic drivers of wheat growth and yield formation. Appropriate tillage can modify soil bulk density and nutrient distribution, thereby affecting the soil environment for root growth [8,9]. Nitrogen management strongly regulates photosynthetic capacity, biomass production, N uptake, and grain yield, with field experiments in winter wheat consistently showing that moderate N inputs achieve better growth, N uptake, and productivity than either insufficient or excessive application [10,11]. Nevertheless, the optimal N rate depends largely on whether the soil environment enables roots to fully capture water and nutrients [12]. Conventional rotary tillage, though effective for seedbed preparation, disturbs only the topsoil and exacerbates compaction at 15–20 cm depth, impeding root elongation and nutrient acquisition [13]. In contrast, conservation tillage practices, especially reduced and no-tillage, as well as subsoiling, are increasingly regarded as more sustainable alternatives [14]. Recent studies have shown that no-tillage can improve yield and nitrogen use efficiency (NUE) under dryland conditions, particularly when combined with residue retention [15], although long-term absence of mechanical loosening may increase surface compaction [16]. Subsoiling loosens the soil to 30–40 cm without inverting the soil profile, thereby breaking the plow pan and improving pore connectivity [16,17], which has positive effects on wheat yield and resource-use efficiency [6,18]. Nevertheless, the agronomic performance of conservation tillage is highly dependent on environmental conditions and crop management, particularly nitrogen supply [19]. The coupled effects of tillage and N application rate, and the underlying mechanisms regulating grain yield and NUE in winter wheat, remain insufficiently understood.

Root system architecture, characterized by root length density (RLD), root surface area density (RSAD), and root dry weight density (RDWD), is a crucial determinant of water and nitrogen acquisition [20,21]. Modest increases in deep root growth can significantly enhance nitrogen uptake, while tillage practices can reshape root development to alter this capacity [22,23]. Under subsoiling, the alleviation of compaction increases RLD in deeper soil layers, which is associated with improved water uptake during grain filling and enhanced post-anthesis nutrient acquisition [22,24]. The interaction between tillage-induced changes in root distribution and N supply is critical, as N availability can modify root proliferation and architecture through both systemic and local signaling pathways [25]. Once taken up, N assimilation and translocation are regulated by a suite of key enzymes, among which nitrate reductase (NR), glutamine synthetase (GS), and glutamate pyruvate transaminase (GPT) play central roles [10,26]. The coordinated regulation of these enzyme activities in roots, leaves, and developing grains is essential for efficient nitrogen utilization and grain protein accumulation [27]. While tillage and nitrogen management can differentially affect both root morphological traits and enzyme activities in different organs [25,28], their combined effects on these belowground and aboveground physiological processes still warrant further validation, particularly under the specific cropping systems of the North China Plain.

Although root functional traits and optimized tillage–nitrogen management are important for improving wheat productivity [22,29], the mechanistic links among tillage-induced changes in root architecture, nitrogen-metabolizing enzyme activities, and yield formation are not yet fully understood. This knowledge gap is particularly relevant to the winter wheat–summer maize system of the North China Plain, where integrated evaluations across

contrasting tillage practices and N application rates remain limited. We hypothesized that, compared with rotary tillage and no-tillage, subsoiling would enhance root proliferation, post-anthesis N uptake, and N-assimilating enzyme activities. These responses were expected to enable a lower N input than the conventional rate to maintain grain yield in the North China Plain. To test this hypothesis, a two-year field experiment was conducted with three tillage practices and three N application rates. The objectives were to (i) quantify the individual and interactive effects of tillage and N rate on grain yield and NUE; (ii) elucidate the underlying mechanisms by examining root growth and the activities of key N-metabolizing enzymes in different plant organs; and (iii) determine whether subsoiling with a reduced N rate can sustain grain yield and improve NUE compared to conventional high-N practices, thereby identifying a suitable tillage–N management strategy in this region.

2. Materials and Methods

2.1. Site Description

This study was conducted during the 2022–2023 and 2023–2024 wheat growing seasons at the Gaocheng Experiment Station of Hebei Agricultural University, China (38°15′ N, 114°45′ E). The soil at the experimental site is a loam. Prior to sowing, the bulk density of the 0–20 cm soil layer was 1.45 g cm^{-3}, and the average bulk density of the 0–200 cm soil profile was 1.56 g cm^{-3}. The initial soil fertility in the 0–20 cm layer before sowing was as follows: alkali-hydrolyzable nitrogen, 129.0 mg kg^{-1}; available potassium, 149.5 mg kg^{-1}; available phosphorus, 17.6 mg kg^{-1}; total nitrogen, 1.03 g kg^{-1}; and soil organic matter, 18.8 g kg^{-1}. Based on China's official soil fertility classification criteria, the topsoil of the experimental site had a moderate level of organic matter, relatively abundant total N, abundant alkali-hydrolyzable N, and relatively abundant available K and available P (Table S1). During the 2022–2023 wheat growing season, the mean daily temperature was 11.22 °C and the total precipitation was 106.1 mm. During the 2023–2024 wheat growing season, the mean daily temperature was 11.25 °C and the total precipitation was 63.8 mm. The seasonal distributions of monthly precipitation and mean temperature are shown in Figure 1.

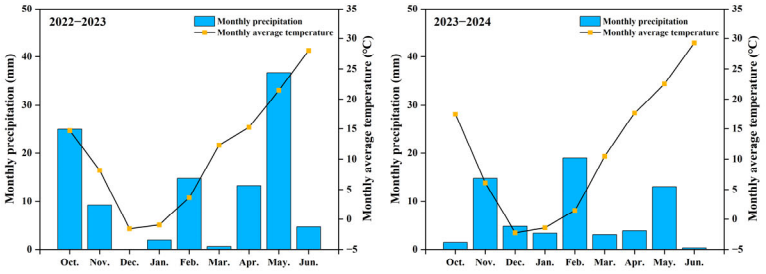

Figure 1. Monthly precipitation and mean temperature during the 2022–2023 and 2023–2024 wheat growing seasons.

2.2. Experimental Design and Management

The wheat cultivar Jimai 22 was used in this study. A two-factor split-plot design was adopted, with tillage practice (T) as the main-plot factor and nitrogen (N) application rate as the subplot factor. Three tillage treatments were established: rotary tillage (R, conventional tillage), subsoiling (S), and no-tillage (Z). Three N application rates were applied in the subplots: 120 kg ha^{-1} (N120), 180 kg ha^{-1} (N180), and 240 kg ha^{-1} (N240). The tillage treatments were implemented according to the method described by Wang [14]. The subsoiling treatment was performed biennially, conducted only on 13 October 2022

before the first growing season. In contrast, rotary tillage and no-tillage operations were conducted annually before sowing in both growing seasons. For the subsoiling treatment, a subsoiler (Shandong Tiansheng Machinery Technology Co., Ltd., Dezhou, China) was used to a depth of 30–35 cm. For the rotary tillage treatment, a rotary cultivator (Hebei Nonghaha Machinery Co., Ltd., Shijiazhuang, China) was used to a depth of 10–15 cm.

All fertilizers were broadcast-applied. Nitrogen fertilizer was supplied as urea (46.4% N), phosphorus fertilizer as triple superphosphate (46% P_2O_5), and potassium fertilizer as potassium chloride (60% K_2O). Phosphorus (135 kg P_2O_5 ha^{-1}) and potassium (150 kg K_2O ha^{-1}) were applied entirely as basal fertilizers before sowing. Urea was applied at a basal-to-topdressing ratio of 1:1, with half applied before sowing and the remaining half topdressed at the jointing stage together with irrigation. Irrigation was applied in fixed amounts, with a total seasonal irrigation amount of 120 mm, including 60 mm at the jointing stage and 60 mm at anthesis. Each plot measured 40 m in length and 2 m in width, with 1 m buffer zones planted with wheat between adjacent plots to prevent lateral water seepage. To avoid edge effects, the outer two rows and 0.5 m at both ends of each plot were excluded from all sampling and yield determination. All treatments were replicated three times. In the 2022–2023 growing season, wheat was sown on 15 October 2022 and harvested on 11 June 2023. In the 2023–2024 growing season, wheat was sown on 10 October 2023 and harvested on 11 June 2024. After the preceding maize was harvested, all maize straw was chopped and returned to the soil. Sowing was carried out with a row spacing of 15 cm. The initial sowing rate was 235 kg ha^{-1}, based on the thousand-grain weight and germination rate of the seed lot. At the three-leaf stage, seedlings were thinned to establish a plant density of 450 plants m^{-2}. Thinning was conducted in all plots using the same criterion and was intended to reduce variation in plant establishment and ensure a comparable initial plant population among treatments. Thus, the same initial sowing rate and final plant-density target were maintained across all tillage and nitrogen treatments.

Weeds, insect pests, and diseases were managed uniformly across all plots to avoid confounding treatment effects. The herbicide florasulam was applied at the regreening stage. The fungicide tebuconazole was applied at the jointing and booting stages to control stripe rust, leaf rust, and powdery mildew. The insecticide thiamethoxam was applied at the heading stage to control cereal aphids. All agrochemicals were applied at their recommended rates, with identical management practices implemented across all plots regardless of tillage practice or N application rate. Other field management practices were consistent with those used in local high-yield wheat production fields.

2.3. Measurements and Methods

2.3.1. Grain Yield and Yield Components

At maturity, wheat grain was harvested to determine yield and yield components. Grain yield was determined by harvesting three randomly selected 1.8 m^2 quadrats from the interior of each plot, giving a total harvested area of 5.4 m^2 per plot. In each plot, spike number was investigated in 1 m of two adjacent rows, with the measurement replicated three times per plot at randomly selected locations. The mean value was then used to calculate the number of spikes per hectare. Fifty representative spikes were continuously sampled from each plot to determine grain number per spike. Grain yield and thousand-grain weight were adjusted to a standard moisture content of 12.5%.

2.3.2. Dry Matter Accumulation and Remobilization

At the anthesis and maturity stages, 15 representative plants were sampled from each plot. The mean dry matter accumulation per plant was then converted to an area basis using the plant density determined for the corresponding sampling occasion. At anthesis,

plant samples were separated into stem + sheath, leaf, and rachis + glumes; at maturity, they were separated into stem + sheath, leaf, rachis + glumes, and grain. Plant density at each sampling occasion was determined by counting plants in two adjacent rows over a 1 m length at three randomly selected locations in each plot, following the same procedure used for spike-number determination. Plant samples were first heated at 105 °C for 30 min to deactivate enzymes and then dried at 80 °C to constant weight in a forced-air oven. Dry weight was then recorded. The remobilization of pre-anthesis reserves, post-anthesis dry matter accumulation, and their contribution to grain were calculated following Zhu et al. [30]:

$$\text{Organ DMA} = \text{DMA per plant} \times \text{plant density} \times 10^{-3} \quad (1)$$

$$\text{DMA}_{\text{anthesis}} = \text{DMA}_{\text{stem+sheath}} + \text{DMA}_{\text{leaf}} + \text{DMA}_{\text{rachis+glumes}} \text{ at anthesis} \quad (2)$$

$$\text{DMA}_{\text{maturity}} = \text{DMA}_{\text{stem+sheath}} + \text{DMA}_{\text{leaf}} + \text{DMA}_{\text{rachis+glumes}} + \text{DMA}_{\text{grain}} \text{ at maturity} \quad (3)$$

$$\text{PRT} = \text{DMA}_{\text{anthesis}} - \text{DMA}_{\text{maturity}} \text{ in vegetative organs} \quad (4)$$

$$\text{POA} = \text{DMA}_{\text{maturity}} - \text{DMA}_{\text{anthesis}} \quad (5)$$

$$\text{CPRT} = \frac{\text{PRT}}{\text{DMA}_{\text{grain}} \text{ at maturity}} \times 100\% \quad (6)$$

$$\text{CPOA} = \frac{\text{POA}}{\text{DMA}_{\text{grain}} \text{ at maturity}} \times 100\% \quad (7)$$

where DMA is dry matter accumulation (kg ha^{-1}), DMA per plant is dry matter accumulation per plant (g plant^{-1}), plant density is expressed as plant ha^{-1}, PRT is the remobilization of pre-anthesis reserves (kg ha^{-1}), POA is the post-anthesis dry matter accumulation (kg ha^{-1}), CPRT is the contribution of PRT to grain yield (%), and CPOA is the contribution of POA to grain yield (%).

2.3.3. Nitrogen Accumulation and Translocation

Dry matter samples of anthesis and maturity stages were ground and analyzed for nitrogen concentration. After digestion with H_2SO_4–H_2O_2 using a digestion furnace, the total plant nitrogen content was determined using a continuous flow autoanalyzer (Futura 2, Italy). Nitrogen accumulation and translocation parameters, including nitrogen uptake efficiency (NUpE), nitrogen utilization efficiency (NUtE), nitrogen harvest index (NHI), and partial factor productivity of nitrogen (PFPN), were calculated according to Li et al. [22] as follows:

$$\text{NUpE} = \frac{U}{F} \quad (8)$$

$$\text{NUtE} = \frac{Y}{U} \quad (9)$$

$$\text{NHI} = \frac{Gn}{U} \times 100\% \quad (10)$$

$$\text{PFPN} = \frac{Y}{F} \quad (11)$$

where U is the total aboveground N uptake at maturity (kg ha^{-1}), F is the N application rate (kg ha^{-1}), Y is the grain yield, and Gn is the grain N accumulation (kg ha^{-1}).

2.3.4. Root Sampling and Root Growth Parameter Analysis

At the booting stage of the 2023–2024 growing season, three root cores were collected from each of the 0–20 and 20–40 cm soil layers in each plot using a root auger (inner diameter, 9 cm). The three cores per plot and soil layer were pooled into a single composite

sample, and the plot was treated as the experimental unit to avoid pseudoreplication. After washing, the roots were gently blotted dry with absorbent paper, and fresh weight (FW) was determined with a precision balance (0.001 g). Roots were then spread out in a transparent tray filled with water, and images were acquired with a flatbed scanner (EPSON Expression V11000XL, Seiko Epson Corporation, Suwa-shi, Nagano-ken, Japan) and analyzed using WinRHIZO software (v.2020a) to determine root diameter, length, surface area, and volume. Samples were then oven-dried at 105 °C for 30 min and subsequently at 80 °C to constant weight to obtain dry weight. RLD, RDWD, and RSAD were calculated as follows [31]:

$$\mathrm{RLD} = \frac{L}{V} \tag{12}$$

$$\mathrm{RDWD} = \frac{G}{V} \tag{13}$$

$$\mathrm{RSAD} = \frac{SR}{V} \tag{14}$$

where RLD is root length density (cm cm^{-3}), RDWD is root dry weight density (10^{-4} g cm^{-3}), RSAD is root surface area density (cm^2 cm^{-3}), V is the volume of the sampled soil (1271.7 cm^3), L is total root length (cm), G is total root dry weight (g), and SR is total root surface area (cm^2).

2.3.5. Determination of Plant Nitrogen Metabolism Enzymes

Key nitrogen-metabolism enzyme activities were determined using plant samples collected during the 2023–2024 growing season. At the booting stage, 10 flag leaves and approximately 5 g of roots collected from the 0–20 cm soil layer were sampled from representative, uniformly growing plants in each plot and pooled to form one composite sample per plot. At the grain-filling stage, plants that reached anthesis on the same day were tagged. Subsequently, 10 flag leaves, approximately 5 g of roots from the 0–20 cm soil layer, and five uniform spikes were collected from the tagged plants and pooled to form one composite sample per plot. All samples were immediately frozen in liquid nitrogen and stored at −80 °C until analysis. Each plot was considered one biological replicate, with three biological replicates analyzed for each treatment and sampling stage.

NR, GS, and GPT activities were determined according to the methods described in [26,32], with minor modifications. NR activity was determined by measuring nitrite production. Approximately 0.2 g FW of plant tissue was homogenized in phosphate buffer (pH 7.5), and the homogenates were centrifuged at 12,000× g for 20 min. In total, 0.4 mL of the clarified extract was incubated in the dark at 25 °C for 30 min with 1.4 mL of reaction mixture containing 100 mM KNO_3 and 0.25 mM NADH. Color development was initiated by adding equal volumes of 1% (w/v) sulfanilamide in 3 M HCl and 0.02% (w/v) N-(1-naphthyl) ethylenediamine. After incubation at room temperature for 15 min, absorbance was measured at 540 nm. NR activity was expressed as μmol NO_2^- g^{-1} FW h^{-1}.

GS activity was determined using the γ-glutamylhydroxamate colorimetric method. Approximately 0.2 g FW of plant tissue was homogenized in phosphate buffer (pH 7.2), and the homogenates were centrifuged at 20,000× g for 20 min. The resulting supernatants were collected for enzyme assays. The enzyme extract was incubated at 25 °C for 30 min with a reaction mixture containing 0.5 mol L^{-1} $MgSO_4$, 0.3 mol L^{-1} sodium glutamate, 0.03 mol L^{-1} ATP-Na, 0.25 mol L^{-1} imidazole–HCl, and 1 mol L^{-1} hydroxylamine–HCl (pH 7.0). The reaction was terminated by adding a stopping solution containing 0.122 mol L^{-1} $FeCl_3$, 0.5 mol L^{-1} trichloroacetic acid, and 2 mol L^{-1} HCl. After centrifugation at 15,000× g for 10 min, absorbance was measured at 540 nm. GS activity was expressed as μmol γ-glutamylhydroxamate g^{-1} FW h^{-1}.

GPT activity was determined using the 2,4-dinitrophenylhydrazine colorimetric method. Approximately 0.2 g FW of plant tissue was homogenized in 0.05 M Tris–HCl buffer (pH 7.2). The homogenates were centrifuged at 20,000× *g* for 20 min, and the resulting supernatants were collected for enzyme assays. The enzyme extract was incubated at 25 °C for 20 min in a reaction mixture containing 200 mM DL-alanine and 2 mM α-ketoglutarate. The reaction was terminated by adding 0.5 mL of 2,4-dinitrophenylhydrazine solution, and absorbance was measured at 505 nm. GPT activity was expressed as μmol pyruvate g^{-1} FW h^{-1}.

2.4. Statistical Analysis

Data from the 2022–2023 and 2023–2024 growing seasons were analyzed separately using a linear mixed-effects model for a split plot design, with tillage as the main-plot fixed factor and N application rate as the subplot fixed factor. Block and the block × tillage interaction were included as random effects, with the block × tillage interaction serving as the main-plot error term for testing the tillage effect. The subplot residual error was used to test the effects of N application rate and the tillage × N application rate interaction. Treatment means within each growing season were compared using Fisher's least significant difference (LSD) test at the 0.05 probability level. Data were organized using Microsoft Excel 2021 and statistically analyzed using SPSS 26.0. Figures were prepared using Origin 2018.

3. Results

3.1. Grain Yield and Yield Components Under Tillage and N Treatments

As shown in Table 1, tillage (T) and nitrogen (N) rate significantly affected grain yield, spike number, grain number per spike, and thousand-grain weight. In both growing seasons, grain yield increased with increasing N rate. The 240 kg N ha^{-1} treatment produced the highest yield. Subsoiling (S) showed a clear advantage over rotary (R) tillage and no-tillage (Z) in improving grain yield and most yield components. Although the T × N interaction was not significant, the highest grain yields in 2022–2023 were observed under SN240 and SN180, reaching 8456.78 and 8129.64 kg ha^{-1}, respectively, with no significant difference between the two treatments. A similar result was observed in 2023–2024, when grain yield was 7940.27 kg ha^{-1} under SN240 and 7700.89 kg ha^{-1} under SN180 (Table S2).

3.2. Accumulation and Remobilization of Dry Matter

At maturity, dry matter accumulation followed the order of grain > stem + sheath > rachis + glumes > leaf in both growing seasons (Figure 2). Subsoiling consistently increased dry matter accumulation across N rates, with the most pronounced effects in grain and leaves. By comparison, higher N rates increased total biomass but shifted its allocation among organs (Table S3). In 2022–2023, grain dry matter accumulation was highest under SN240 with no significant difference from SN180. SN180 showed relatively higher accumulation of leaf and stem + sheath dry matter, reaching 1317.64 and 3335.76 kg ha^{-1}, respectively, while rachis + glumes dry matter was lower than that of RN180 and ZN180. In 2023–2024, SN180 produced the highest leaf dry matter accumulation, reaching 1417.98 kg ha^{-1}. Overall, under subsoiling, reducing the N rate from 240 to 180 kg ha^{-1} significantly increased dry matter accumulation in leaves and decreased that of stem + sheath.

Table 1. Yield and yield components during the 2022–2023 and 2023–2024 growing seasons.

Year	Treatment		Grain Yield (kg ha^{-1})	Spikes (10^4 ha^{-1})	Grain Number per Spike	Thousand-Grain Weight (g)
2022–2023	Tillage (T)	R	7182.82 b	609.54 b	32.13 a	41.37 b
		S	7839.9 a	653.71 a	32.54 a	42.7 a
		Z	6945.96 b	603.76 b	32.45 a	40.91 c
	Nitrogen (N)	N120	6610.45 c	586.2 c	31.17 c	42.03 a
		N180	7496.58 b	630.03 b	32.65 b	42.16 a
		N240	7861.65 a	650.78 a	33.3 a	40.79 b
ANOVA	Tillage (T)		**	**	ns	**
	Nitrogen (N)		**	**	**	**
	T × N		ns	ns	ns	ns
2023–2024	Tillage (T)	R	7039.75 b	611.96 b	34.58 ab	43.11 b
		S	7448.49 a	660.59 a	34.97 a	45.09 a
		Z	6827.78 c	601.52 b	34.39 b	42.88 b
	Nitrogen (N)	N120	6413.48 c	575.56 c	33.55 c	44.6 a
		N180	7218.48 b	636.89 b	34.73 b	43.8 b
		N240	7683.86 a	661.62 a	35.65 a	42.68 c
ANOVA	Tillage (T)		**	*	ns	**
	Nitrogen (N)		**	**	**	**
	T × N		ns	ns	ns	ns

R, rotary tillage; S, subsoiling; Z, no-tillage; N120, N180, and N240 indicate N application rates of 120, 180, and 240 kg ha^{-1}, respectively. Different lowercase letters within the same column and growing season indicate significant differences among treatments ($p < 0.05$). * and ** represent the significance at $p < 0.05$ and $p < 0.01$, respectively; ns, not significant.

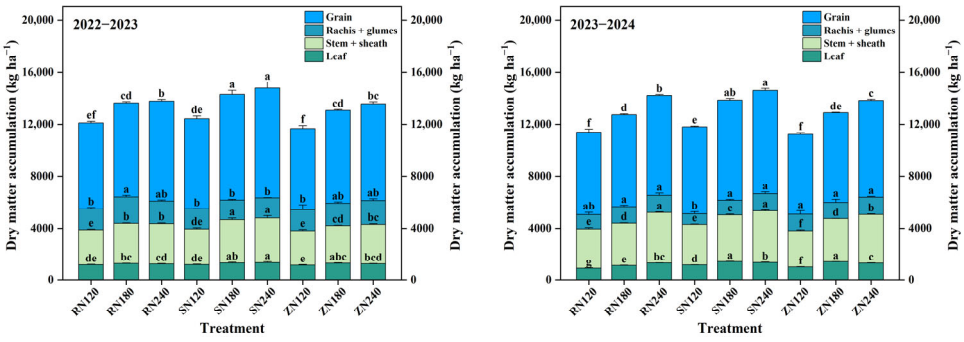

Figure 2. Dry matter accumulation in different organs at maturity during the 2022–2023 and 2023–2024 wheat growing seasons. R, rotary tillage; S, subsoiling; Z, no-tillage; N120, N180, and N240 indicate N application rates of 120, 180, and 240 kg ha^{-1}, respectively. Different lowercase letters on bars of the same color within the same growing season indicate significant differences among treatments ($p < 0.05$).

Across N application rates, subsoiling produced the highest post-anthesis assimilate accumulation and the greatest contribution to grain in both growing seasons (Table 2). When averaged over tillage, N180 and N240 resulted in greater post-anthesis assimilate accumulation than N120. In 2022–2023, under the same tillage practice, the amount of pre-anthesis dry matter remobilization was lower under N120 than under N180 and N240, whereas the contribution of pre-anthesis assimilates to grain was higher under N120. Post-anthesis dry matter accumulation was significantly greater under N180 and N240 than that under N120. Among all treatments, SN180 and SN240 increased post-anthesis dry matter accumulation by 11.22–38.96% and 13.25–41.48%, respectively. Under the same nitrogen rate, the contribution of pre-anthesis assimilates followed the order rotary

tillage > no-tillage > subsoiling, whereas post-anthesis assimilate allocation followed the order subsoiling > rotary tillage > no-tillage. Similar trends were observed for the pre-anthesis dry matter remobilization and post-anthesis assimilate accumulation in the 2023–2024 growing season. At the individual-treatment level, SN180 and SN240 showed the highest post-anthesis dry matter allocation to grain in both growing seasons, with 5500 and 5600 kg ha^{-1} in 2022–2023, and 4657 and 4638 kg ha^{-1} in 2023–2024, respectively (Table S4). SN180 tended to show a relatively high contribution of post-anthesis dry matter to grain in both growing seasons, being numerically 2.16–7.00% higher in 2022–2023 and 3.36–8.34% higher in 2023–2024 than the other treatment combinations.

Table 2. Pre-anthesis assimilate translocation from vegetative organs and post-anthesis assimilate accumulation in grain during the 2022–2023 and 2023–2024 wheat growing seasons.

Year	Tillage	Nitrogen	Pre-Anthesis Reserves		Post-Anthesis Assimilates	
			Translocation to Grain (kg ha^{-1})	Contribution to Grain (%)	Allocation to Grain (kg ha^{-1})	Contribution to Grain (%)
2022–2023	Tillage (T)	R	2540.35 a	35.38 a	4642.48 b	64.62 b
		S	2646.53 a	33.84 b	5193.37 a	66.16 a
		Z	2536.78 a	36.53 a	4409.18 c	63.47 b
	Nitrogen (N)	N120	2385.56 c	36.11 a	4224.89 c	63.89 b
		N180	2564.47 b	34.29 b	4932.11 b	65.71 a
		N240	2773.63 a	35.34 a	5088.02 a	64.66 b
ANOVA	Tillage (T)		ns	**	**	**
	Nitrogen (N)		**	**	**	**
	T × N		ns	ns	*	ns
2023–2024	Tillage (T)	R	2465.04 a	38.20 a	3987.59 b	61.80 b
		S	2436.33 a	35.73 b	4390.96 a	64.27 a
		Z	2353.65 b	37.66 ab	3904.69 b	62.34 ab
	Nitrogen (N)	N120	2241.75 c	38.16 a	3637.02 c	61.84 b
		N180	2373.18 b	35.93 b	4243.28 b	64.07 a
		N240	2640.09 a	37.50 a	4402.94 a	62.50 b
ANOVA	Tillage (T)		**	ns	**	ns
	Nitrogen (N)		**	**	**	**
	T × N		ns	ns	*	ns

R, rotary tillage; S, subsoiling; Z, no-tillage; N120, N180, and N240 indicate N application rates of 120, 180, and 240 kg ha^{-1}, respectively. Different lowercase letters within the same column and growing season indicate significant differences among treatments ($p < 0.05$). * and ** represent the significance at $p < 0.05$ and $p < 0.01$, respectively; ns, not significant.

3.3. Nitrogen Remobilization and Post-Anthesis Uptake

In both growing seasons, increasing nitrogen application promoted the translocation of pre-anthesis nitrogen reserves to grain and post-anthesis nitrogen uptake, whereas the contribution of pre-anthesis reserves to grain generally declined (Table 3). Under the same tillage treatment, N240 usually exhibited the highest pre-anthesis nitrogen translocation and post-anthesis nitrogen uptake, while N120 had the highest contribution of pre-anthesis reserves to grain. Among tillage treatments, no-tillage generally resulted in lower post-anthesis nitrogen uptake. Subsoiling promoted post-anthesis nitrogen uptake and its contribution to grain, with values of 54.92 kg ha^{-1} and 23.18% in 2022–2023, and 36.1 kg ha^{-1} and 17.45% in 2023–2024, respectively. SN240 recorded the highest pre-anthesis N translocation to grain, whereas SN180 was 7.91–9.43% lower during the two growing seasons (Table S5). SN180 showed a more balanced nitrogen supply pattern than the other treatments. In 2022–2023, SN180 achieved 185.03 kg ha^{-1} of pre-anthesis

nitrogen translocation to grain, and 55.68 kg ha^{-1} of post-anthesis nitrogen uptake, with a 23.13% contribution of post-anthesis nitrogen uptake to grain, all of which were markedly higher than those of the corresponding RN180 and ZN180 treatments. A similar trend was observed in 2023–2024, indicating that subsoiling with 180 kg N ha^{-1} tended to improve the coordination between nitrogen remobilization and post-anthesis nitrogen assimilation.

Table 3. Post-anthesis nitrogen remobilization and uptake during the 2022–2023 and 2023–2024 wheat growing seasons.

Year	Tillage	Nitrogen	Pre-Anthesis Reserves		Post-Anthesis Assimilates	
			Translocation to Grain (kg ha^{-1})	Contribution to Grain (%)	Nitrogen Uptake After Anthesis (kg ha^{-1})	Contribution Rate to Grain (%)
2022–2023	Tillage (T)	R	162.95 b	78.99 a	43.73 b	21.01 a
		S	180.65 a	76.82 a	54.92 a	23.18 a
		Z	168.62 b	80.14 a	42.38 b	19.86 a
	Nitrogen (N)	N120	144.40 c	80.39 a	35.42 c	19.61 b
		N180	170.95 b	78.07 b	48.18 b	21.93 a
		N240	196.87 a	77.48 b	57.43 a	22.52 a
ANOVA	Tillage (T)		**	ns	*	ns
	Nitrogen (N)		**	**	**	**
	T × N		**	ns	ns	ns
2023–2024	Tillage (T)	R	161.34 b	85.21 a	28.27 b	14.79 b
		S	169.27 a	82.55 b	36.10 a	17.45 a
		Z	161.26 b	86.71 a	25.16 b	13.29 b
	Nitrogen (N)	N120	149.58 c	86.99 a	22.55 c	13.01 c
		N180	163.55 b	84.50 b	30.17 b	15.50 b
		N240	178.75 a	82.98 c	36.82 a	17.02 a
ANOVA	Tillage (T)		**	**	**	**
	Nitrogen (N)		**	**	**	**
	T × N		*	ns	ns	ns

R, rotary tillage; S, subsoiling; Z, no-tillage; N120, N180, and N240 indicate N application rates of 120, 180, and 240 kg ha^{-1}, respectively. Different lowercase letters within the same column and growing season indicate significant differences among treatments (p< 0.05). * and ** represent the significance at $p < 0.05$ and $p < 0.01$, respectively; ns, not significant.

3.4. Nitrogen Use Efficiency and Associated Parameters

In both growing seasons, NUpE decreased progressively with increasing N rate under all tillage treatments, with N120 showing the highest values and N240 the lowest (Figures 3 and 4, Table S6). Under the same N rate, subsoiling produced the highest NUpE, reaching 1.33 and 1.50 kg kg^{-1} in 2022–2023 and 2023–2024. SN180 achieved NUpE values of 1.29 and 1.46 kg kg^{-1} in the 2022–2023 and 2023–2024 growing seasons, respectively. These values were 19.8% and 21.6% lower than those of SN120, and 17.7% and 21.9% higher than those of SN240, respectively. NUtE was highest under RN120 and generally declined as N rate increased. SN180 maintained a moderate NUtE of 29.34–34.99 kg kg^{-1} in both growing seasons, with no significant difference from SN120 or SN240.

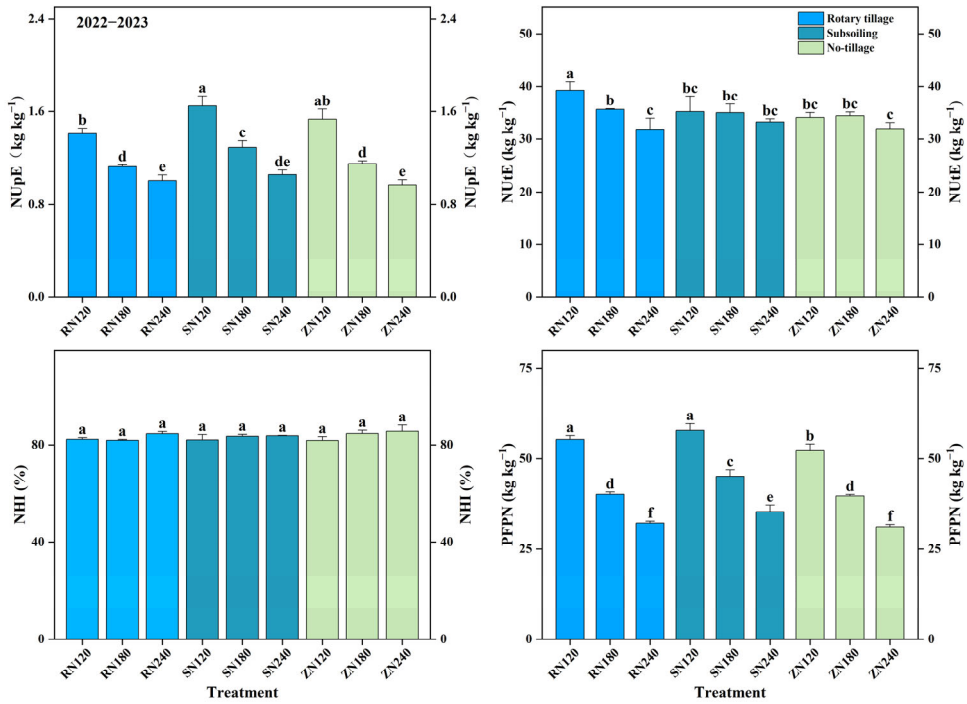

Figure 3. Nitrogen use efficiency and associated parameters during the 2022–2023 wheat growing season. NUpE, nitrogen uptake efficiency; NUtE, nitrogen utilization efficiency; NHI, nitrogen harvest index; PFPN, partial factor productivity of nitrogen fertilizer. R, rotary tillage; S, subsoiling; Z, no-tillage; N120, N180, and N240 indicate N application rates of 120, 180, and 240 kg ha^{-1}, respectively. Different lowercase letters above bars indicate significant differences among treatments ($p < 0.05$).

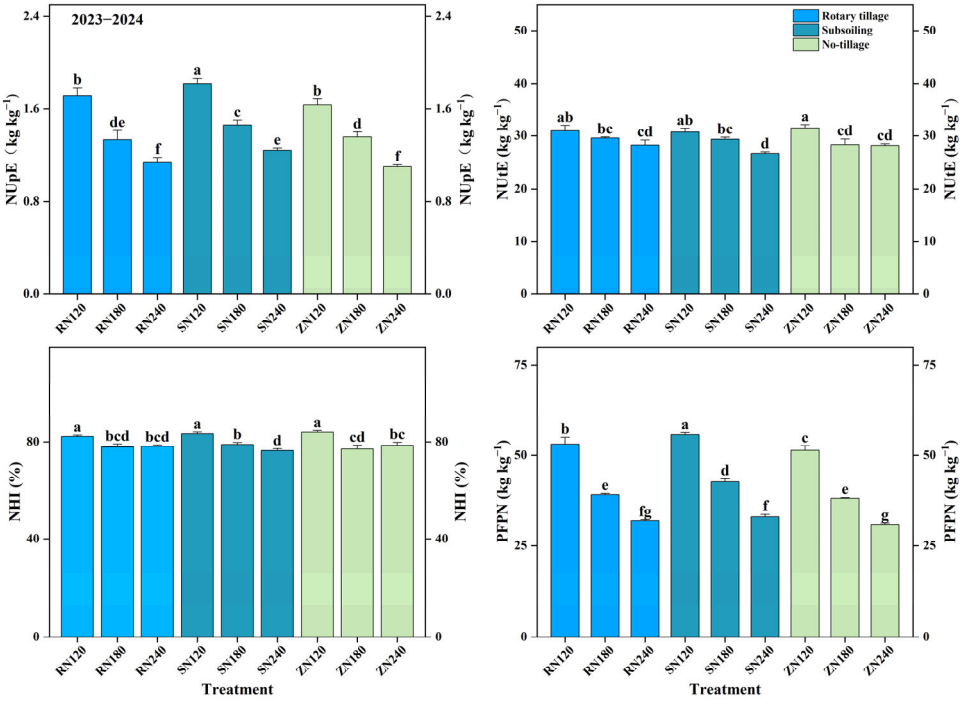

Figure 4. Nitrogen use efficiency and associated parameters during the 2023–2024 wheat growing season. NUpE, nitrogen uptake efficiency; NUtE, nitrogen utilization efficiency; NHI, nitrogen harvest index; PFPN, partial factor productivity of nitrogen fertilizer. R, rotary tillage; S, subsoiling; Z, no-tillage; N120, N180, and N240 indicate N application rates of 120, 180, and 240 kg ha^{-1}, respectively. Different lowercase letters above bars indicate significant differences among treatments ($p < 0.05$).

NHI ranged from 81.84% to 85.57% in 2022–2023 and from 76.35% to 84.04% in 2023–2024. No significant effects of tillage or tillage × N rate interaction on NHI were observed. PFPN decreased significantly with increasing N rate across all tillage treatments. Under the same N rate, subsoiling consistently achieved the highest PFPN values. SN180 recorded PFPN values of 45.16 kg kg^{-1} and 42.78 kg kg^{-1} in both growing seasons. Compared with SN240, SN180 increased PFPN by 28.2–29.3%. Across both growing seasons, subsoiling combined with 180 kg N ha^{-1} consistently balanced relatively high NUpE, moderate NUtE, and competitive PFPN, while maintaining a stable NHI. This combination achieved superior N efficiency compared with rotary tillage and no-tillage at the same N rate, without the substantial declines in NUtE and PFPN observed under N240.

3.5. Root Growth and Morphological Parameters at the Booting Stage

In the 2023–2024 growing season, RLD, RSAD, RDWD, and mean root diameter were measured in the 0–20 cm and 20–40 cm soil layers at the booting stage (Figure 5). In general, root growth was more active in the 0–20 cm soil layer than in the 20–40 cm soil layer. Tillage and N application rate significantly affected RLD, RSAD, and RDWD, while root diameter showed little variation among treatments (Table S7). In the upper layer, RLD ranged from 1.79 to 4.19 cm cm^{-3}, with the highest value observed under ZN240. In the 20–40 cm layer, SN180 achieved the highest RLD of 2.40 cm cm^{-3}. Under N180, subsoiling increased RLD by 41.8% and 59.7% compared with rotary tillage and no-tillage, respectively. RSAD showed a similar vertical distribution. ZN240 recorded the highest RSAD of 18.49 cm^2 cm^{-3} in the 0–20 cm layer, while SN180 had the highest RSAD of 8.23 cm^2 cm^{-3}.

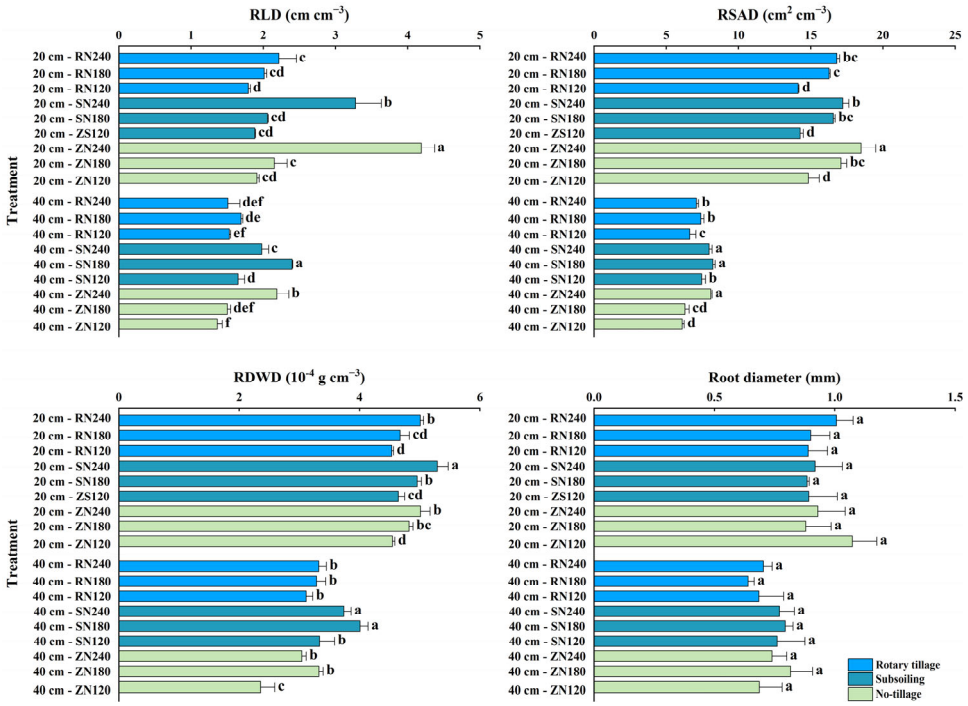

Figure 5. Root growth and morphological parameters at the booting stage during the 2023–2024 wheat growing season. RLD, root length density; RSAD, root surface area density; RDWD, root dry weight density. R, rotary tillage; S, subsoiling; Z, no-tillage; N120, N180, and N240 indicate N application rates of 120, 180, and 240 kg ha^{-1}, respectively. Different lowercase letters above bars within the same soil layer indicate significant differences among treatments ($p < 0.05$).

RDWD followed similar trends, while the highest value was observed under SN240 in the 0–20 cm layer, which was 5.29 mg cm^{-3}. In the deeper layer, SN180 treatment produced the highest RDWD of 4.01 mg cm^{-3}, significantly greater than other treatments except for

SN240. RDWD was 22.0% and 20.5% higher under SN180 than under RN180 and ZN180, respectively. Root diameter did not differ significantly among treatments within either soil layer, ranging from 0.64 to 1.07 mm.

3.6. Nitrogen Metabolism Enzyme Activities

In the 2023–2024 growing season, plant tissues were sampled at the booting and grain-filling stages for the determination of key nitrogen-metabolizing enzyme activities. At the booting stage, the activities of NR, GS, and GPT showed clear treatment-dependent differences (Figure 6). In flag leaves, NR activity increased progressively with N rate under all tillage treatments (Table S8). N180 and N240 showed significantly higher NR activities than N120, while no significant differences were observed between N180 and N240. Under the same N rate, subsoiling and rotary tillage generally outperformed no-tillage. Notably, ZN120 recorded the lowest flag leaf NR activity of 6.76 μmol g^{-1} FW h^{-1}. GS activity exhibited a similar pattern in flag leaves. SN240, RN240, and SN180 achieved the highest GS activities, while no-tillage, regardless of N rate, maintained relatively low GS activities, with ZN180 and ZN240 showing no significant improvement over ZN120. GPT activity in flag leaves was highest under SN240 and SN180, with values of 355.61 and 340.64 μmol g^{-1} FW h^{-1}, respectively.

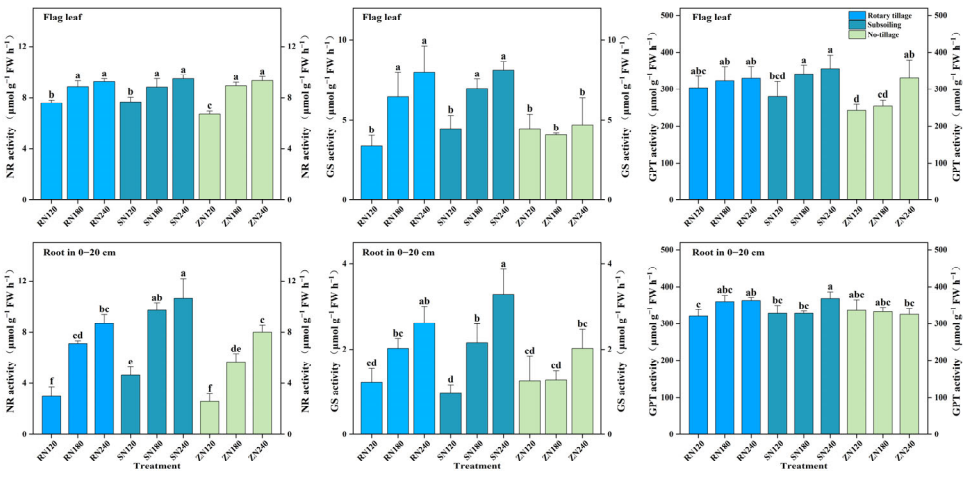

Figure 6. Nitrogen metabolism enzyme activities at the booting stage during the 2023–2024 wheat growing season. NR, nitrate reductase; GS, glutamine synthetase; GPT, glutamate pyruvate transaminase. R, rotary tillage; S, subsoiling; Z, no-tillage; N120, N180, and N240 indicate N application rates of 120, 180, and 240 kg ha^{-1}, respectively. Different lowercase letters above bars indicate significant differences among treatments ($p < 0.05$).

In roots, tillage significantly affected GS and NR activities but had no significant effect on GPT activity. Nitrogen application rate significantly increased the activities of all three enzymes (Table S8). SN240 recorded the highest root NR activity, followed by SN180, at 10.65 and 9.68 μmol g^{-1} FW h^{-1}, respectively, both of which were significantly higher than those in all other treatments. SN180 maintained a moderate GS activity of 2.15 μmol g^{-1} FW h^{-1}. Root GPT activity was significantly higher under SN240 and RN240 compared with most N120 and N180 treatments, though the magnitude of differences was smaller than that observed for NR and GS.

At the grain-filling stage, NR, GS, and GPT activities were measured in flag leaves, roots in the 0–20 cm soil layer, and grains (Figure 7, Table S9). In flag leaves, NR activity was highest under the N240 treatments, with RN240 and SN240 recording values of 3.18 and 3.14 μmol g^{-1} FW h^{-1}, respectively. GS activity in flag leaves was significantly enhanced by subsoiling at higher N rates. SN240 and SN180 achieved the highest GS activities at

9.59 and 8.61 μmol g^{-1} FW h^{-1}, respectively, significantly exceeding all rotary tillage and no-tillage treatments. GPT activity in flag leaves also peaked under SN240 and RN240, with both treatments significantly outperforming all N120 treatments. SN180 maintained a flag leaf GPT activity of 461.25 μmol g^{-1} FW h^{-1}, which was significantly higher than those of all N120 treatments and ZN180.

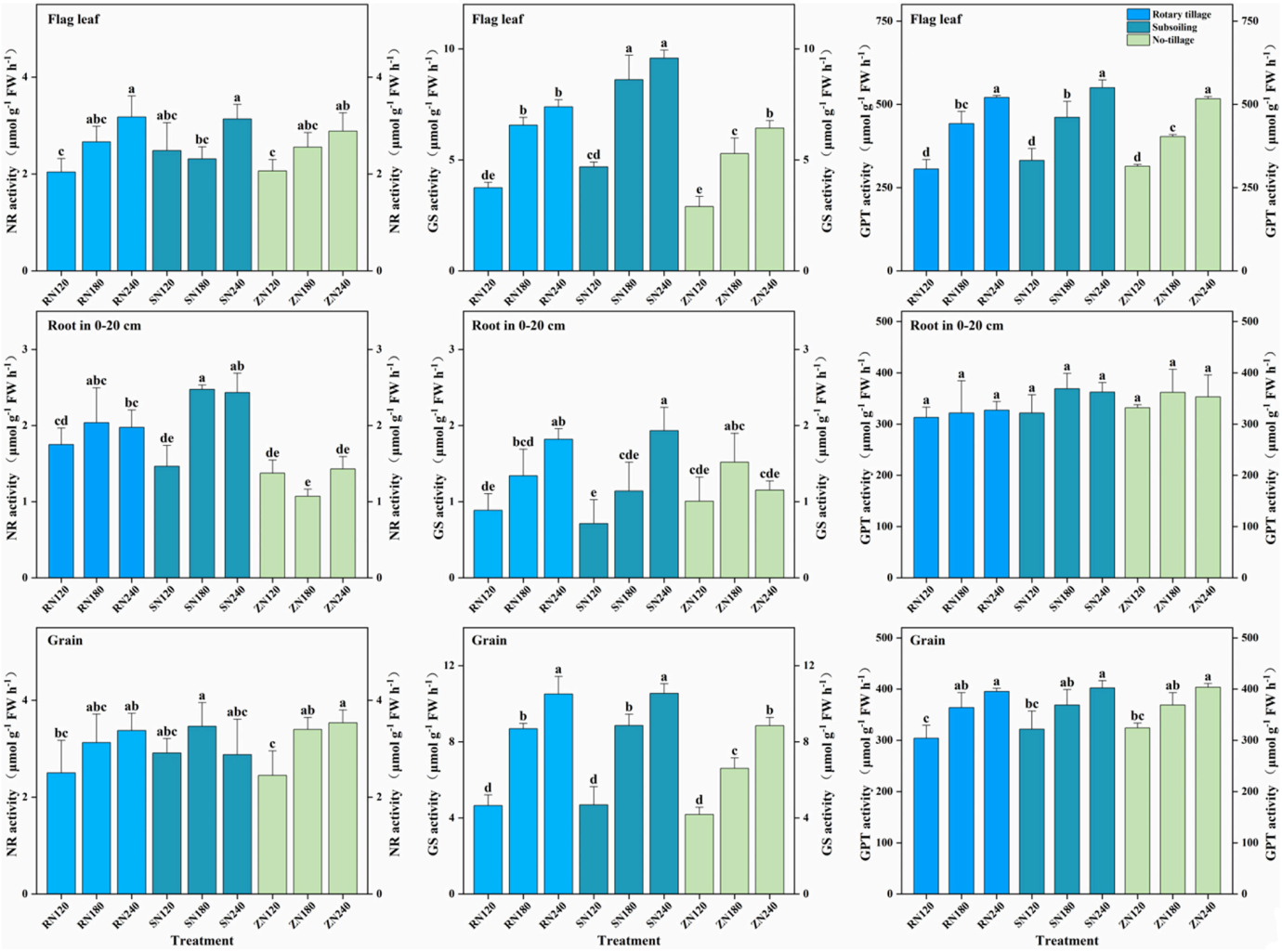

Figure 7. Nitrogen metabolism enzyme activities at the grain-filling stage during the 2023–2024 wheat growing season. NR, nitrate reductase; GS, glutamine synthetase; GPT, glutamate pyruvate transaminase. R, rotary tillage; S, subsoiling; Z, no-tillage; N120, N180, and N240 indicate N application rates of 120, 180, and 240 kg ha^{-1}, respectively. Different lowercase letters above bars indicate significant differences among treatments ($p < 0.05$).

In roots, NR activity was highest under SN180 and SN240 with values of 2.48 and 2.43 μmol g^{-1} FW h^{-1}, which were significantly greater than most other treatments except RN180 and RN240. No-tillage consistently displayed the lowest root NR activities, with ZN180 recording the lowest value of 1.07 μmol g^{-1} FW h^{-1}. Root GS activity followed a similar pattern, with SN240 achieving the highest value of 1.93 μmol g^{-1} FW h^{-1}, significantly exceeding all treatments except RN240. Root GPT activity showed no significant differences among treatments at the grain-filling stage.

In grains, tillage significantly affected GS activity but not GPT or NR activity. Compared with no-tillage, rotary tillage and subsoiling increased GS activity by 21.6% and 22.8%, respectively. The N application rate significantly affected all three enzyme activities. The activities of GS, GPT, and NR increased by 78.9%, 16%, and 27.1%, respectively,

when the N application rate increased from 120 to 180 kg ha^{-1}. N240 treatments exhibited the highest GS activities under all tillage systems, with SN240 and RN240 reaching 10.54 and 10.51 μmol g^{-1} FW h^{-1}, respectively. Grain GS activity under SN180 was 8.85 μmol g^{-1} FW h^{-1}. Grain GPT activity was highest under the N240 treatments across all tillage systems. Meanwhile, SN180 maintained a relatively high grain GPT activity of 369.05 μmol g^{-1} FW h^{-1}. Taken together, subsoiling combined with 180 kg N ha^{-1} consistently enhanced NR and GS activities in flag leaves and roots at the booting stage and sustained relatively high enzyme activities in leaves and grains at the grain-filling stage.

4. Discussion

4.1. Subsoiling with Moderate Nitrogen Application Sustains Grain Yield

Across the two growing seasons, subsoiling generally increased grain yield compared with rotary tillage and no-tillage. Grain yield increased with increasing N rate under all three tillage practices, indicating that N availability remained an important constraint on wheat productivity at the experimental site. However, at the same N rate, subsoiling consistently produced higher grain yield and generally better yield components than rotary tillage and no-tillage treatments. This yield advantage is consistent with previous studies showing that subsoiling can improve crop productivity [33]. In the present study, this advantage was primarily associated with increases in spike number and thousand-grain weight. Although SN240 produced the numerically highest yield, the additional yield benefit of increasing the N rate from 180 to 240 kg ha^{-1} under subsoiling was statistically nonsignificant, demonstrating that subsoiling with 180 kg N ha^{-1} (SN180) maintained comparable yields with a 25% reduction in N input.

Regarding inter-annual variability, the lower precipitation in the 2023–2024 growing season was accompanied by lower grain yield in most treatments, but the relative advantage of subsoiling was maintained. This consistency across two seasons indicates that the yield benefits of subsoiling were reasonably stable. Nevertheless, because both seasons received the same amount of supplemental irrigation, the present findings mainly demonstrate the response under irrigated winter wheat production and should not be directly extended to purely rainfed production systems.

4.2. Subsoiling Improved Yield Formation by Promoting Post-Anthesis Assimilate Production

Dry matter allocation provides further insight into the yield response. In both growing seasons, subsoiling increased post-anthesis assimilate accumulation and its allocation to grain. SN180 consistently showed the highest contribution of post-anthesis assimilates to grain, exceeding the other treatments by 2.16–7.00% in 2022–2023 and 3.36–8.34% in 2023–2024. Under subsoiling practice, the contribution of pre-anthesis reserves tended to be lower. Such a shift is generally favorable because sustained post-anthesis assimilation supports grain filling while slowing depletion of vegetative organs and delaying premature canopy senescence [34]. Recent research has emphasized that the contribution of post-anthesis assimilation to wheat yield depends not only on canopy photosynthetic capacity but also on continued access to water and N during grain filling [35]. The greater post-anthesis dry matter accumulation under subsoiling was therefore consistent with, but did not directly demonstrate, improved late-season resource acquisition. The enhanced root growth in the 20–40 cm soil layer observed in 2023–2024 may partly explain this pattern. Deeper roots can better access resources located below the intensively explored surface layer [36]. Although depth-specific resource uptake was not directly measured, this proposed link remains a plausible biological pathway for the sustained assimilation. Compared with subsoiling, no-tillage produced less post-anthesis dry matter and lower grain yield. Although no-tillage can improve soil structure in some dryland systems, its

effects depend on the duration of implementation and residue management [37]. Under the soil conditions at this site, the limited root proliferation and late-season resource capture were reduced. No-tillage may have been associated with persistent soil mechanical resistance under minimal soil disturbance.

4.3. Subsoiling Coordinated N Remobilization, Post-Anthesis N Uptake, and Nitrogen Use Efficiency

Sustaining grain yield requires coordinated N remobilization from vegetative organs and post-anthesis N uptake. Increasing the N application rate enhanced the absolute amounts of pre-anthesis N translocation and post-anthesis N uptake, with a general reduction in NUpE and partial factor productivity. This pattern reflects the diminishing returns from additional N once crop N demand approaches saturation [38]. At the same N rate, subsoiling generally increased post-anthesis N uptake and its contribution to grain relative to rotary tillage and no-tillage. SN180 maintained substantial pre-anthesis N translocation while also showing relatively high post-anthesis N uptake. The yield increase under SN180 therefore reflected not only enhanced remobilization of N stored in vegetative organs, but also a greater capacity to absorb soil N during grain filling. This is important because excessive reliance on pre-anthesis N remobilization can accelerate the degradation of photosynthetic proteins and shorten the functional duration of leaves, whereas continued post-anthesis uptake helps maintain N supply to developing grains while supporting canopy photosynthesis [39].

Although N120 showed the highest NUpE and PFPN, its lower absolute yield indicated this efficiency was partly a mathematical artifact of the small denominator. Conversely, N240 increased absolute N accumulation and produced the numerically highest yield but reduced fertilizer productivity. Compared with SN240, SN180 represented a more balanced treatment, achieving a 25% reduction in N input while significantly increasing PFPN by 28.2–29.3% and NUpE by 17.7–21.9% in the two growing seasons, respectively. The relatively stable NHI across treatments suggests that tillage and N application rate treatments had a greater influence on total N acquisition than on the proportional partitioning of accumulated N to grain. It should also be noted that the agronomically appropriate N rate varies with soil mineral N supply, target yield, precipitation, cultivar, and crop rotation [38,40]. However, under the conditions of this experiment, these improvements in N acquisition and utilization directly enabled SN180 to sustain high grain yield despite the 25% reduction in N input.

Beyond agronomic productivity, the environmental implications of reducing N input are substantial. In the North China Plain, fertilizer N applied in excess of crop removal is largely lost through nitrate leaching and gaseous emissions, contributing to groundwater nitrate contamination and elevated N_2O fluxes [2]. In the present study, SN180 received 60 kg ha^{-1} less nitrogen than SN240, while returning higher NUpE and PFPN. These findings suggest that SN180 may have lowered the risk of excess residual soil N accumulation. Although leaching and gaseous losses were not measured directly and the magnitude of any environmental benefit therefore cannot be quantified, the pattern is consistent with evidence that moderate N rates in this region reduce nitrate leaching and N_2O emissions relative to higher rates [4,14], supporting more sustainable production.

4.4. Root and Enzymatic Responses Associated with Nitrogen Acquisition

Root system architecture and internal N metabolism are successive and closely connected components of crop N use [35]. To further explain the yield advantage of subsoiling, we examined the underlying root and enzymatic mechanisms during the 2023–2024 growing season. Subsoiling improved N use by enhancing both the physical exploration of soil by roots and the physiological capacity for N assimilation. At the booting stage, subsoiling

increased RLD, RSAD, and RDWD, with a particularly important response in the 20–40 cm layer. These root traits together expanded the potential soil volume explored by roots and may have contributed to greater post-anthesis N acquisition. The greater root development observed below 20 cm is consistent with the expected response to reduced mechanical impedance near or below the shallow cultivated layer [35]. It may also have increased the probability of roots encountering water and mobile nutrients located below the surface layer [35,36]. Although depth-specific resource uptake was not directly measured, this enhanced root development plausibly improved access to subsoil water and nitrate. Root growth responses to N were nonlinear. Insufficient N can restrict root biomass accumulation because of limited assimilate and protein synthesis, whereas excessive N may promote shoot growth at the expense of root proliferation, thereby reducing the carbon allocated per unit of soil explored [41,42]. The relatively favorable root morphology under SN180 indicates that an adequate but not excessive N supply created conditions conducive to both root development and nutrient uptake.

The activities of NR, GS, and GPT provide a physiological link between enhanced root acquisition and improved N utilization [43]. During the 2023–2024 growing season, enhanced activities of these enzymes under subsoiling, especially in combination with N180, indicate a greater potential for nitrate reduction and ammonium assimilation. The responses among organs and growth stages should be interpreted in the context of their distinct physiological roles. The high demand for N during booting is met by active uptake in roots and leaves, with elevated NR and GS activities supporting fast canopy development and spike differentiation [10,44]. After anthesis, N metabolism increasingly involves the remobilization of N from roots and leaves to sustain grain filling. Maintenance of leaf N-assimilation capacity may be beneficial to delay senescence, whereas enzyme activity in spikes reflects the conversion and deposition of imported N in developing kernels [11]. A plausible mechanistic interpretation is that subsoiling may have reduced mechanical impedance in the 20–40 cm soil layer, thereby facilitating root development, as reflected in higher RLD and RDWD. The resulting expansion of the rooting zone likely helped maintain access to subsoil water and nitrate during grain filling. Sustained post-anthesis N uptake, in turn, may have supported the relatively high activities of NR and GS in leaves and roots, thereby extending photosynthetic duration and assimilate supply to developing grains, which contributed to the higher thousand-grain weight and grain yield observed under subsoiling. Although these physiological measurements were made only in the 2023–2024 season, they provide a consistent biological explanation for the yield and N use advantages observed under subsoiling.

4.5. Agronomic Implications and Study Limitations

Taken together, the results indicate that SN180 offered the most favorable balance between grain yield and N use under the conditions of this experiment. Compared with SN240, SN180 reduced N input by 60 kg ha^{-1} with no significant yield loss, while achieving higher PFPN and NUpE. Relative to rotary tillage and no-tillage at the same N rate, subsoiling was associated with greater post-anthesis dry matter production and N uptake. In 2023–2024, it was also associated with greater root growth, particularly in the 20–40 cm soil layer, and relatively high activities of enzymes involved in N assimilation. The principal conclusion supported directly by this experiment is therefore agronomic: under the conditions tested, subsoiling combined with 180 kg N ha^{-1} maintained high wheat yield with less N input than SN240. The proposed pathway involves the potential alleviation of soil mechanical constraints, deeper root exploration, continued N uptake, and greater N-assimilation capacity. This mechanism was not directly demonstrated, although it is biologically plausible and consistent with the observed responses.

The interpretation of these findings should take several limitations into account. Post-treatment soil physical properties, including penetration resistance, bulk density, and soil water content, were not measured, limiting our ability to directly evaluate the proposed mechanism. Meanwhile, root traits and enzyme activities were assessed in only one of the two growing seasons. Root enzyme activities were assayed only on 0–20 cm roots due to the difficulty of obtaining sufficient living tissue from deeper layers [41]. Consequently, the inter-annual consistency of these responses and the functional contribution of subsoil roots remain uncertain. The absence of an N control treatment prevented direct quantification of indigenous soil N supply and residual N from the preceding crop. Because initial soil fertility data cannot substitute for an N-omission treatment due to dynamically seasonal mineralization, the present results represent relative crop responses to fertilizer-N rates rather than an assessment of the site's natural productivity. Additionally, this study did not trace depth-specific N uptake, nor were environmental N losses and economic returns quantified. Moreover, because this experiment was conducted at a single site over two growing seasons, caution should be exercised when extrapolating these results to the broader North China Plain without further multi-site validation.

Despite these limitations, under conditions similar to this study, subsoiling combined with 180 kg N ha^{-1} remains a promising management option for irrigated winter wheat fields affected by long-term shallow tillage in the North China Plain. Longer-term, multi-site studies are needed to determine the persistence, mechanisms, and regional applicability of this management strategy. These studies should integrate soil physical measurements, depth-specific root function, N control treatments to quantify indigenous soil N supply, ^{15}N tracing, environmental N loss assessment, and economic analysis.

5. Conclusions

A two-year field experiment showed that subsoiling increased winter wheat yield, post-anthesis dry matter accumulation, and post-anthesis N uptake relative to rotary tillage and no-tillage. In the 2023–2024 growing season, subsoiling significantly increased RLD, RSAD, and RDWD, especially in the 20–40 cm soil layer, and sustained relatively high activities of NR, GS, and GPT in both roots and aboveground organs, although the magnitude of these effects varied among organs and growth stages. These responses likely strengthened N acquisition and assimilation during the reproductive period and contributed to sustained grain filling.

Subsoiling with 180 kg N ha^{-1} produced grain yields of 8129.64 and 7700.89 kg ha^{-1} in the two growing seasons, with no significant difference from SN240. Compared with SN240, SN180 reduced N input by 25% and increased PFPN and NUpE by 28.2–29.3% and 17.7–21.9%, respectively. It also increased the contribution of post-anthesis assimilates to grain and maintained greater post-anthesis N uptake than the corresponding rotary tillage and no-tillage treatments. Under the conditions of this study, subsoiling combined with 180 kg N ha^{-1} provided the most favorable balance between grain yield and N input among the tested treatments. Soil physical properties were not measured after treatment, and root traits and enzyme activities were determined in only one growing season. The proposed mechanisms could therefore not be evaluated directly. Long-term, multi-site studies incorporating environmental and economic assessments are needed to confirm its broader applicability.

Supplementary Materials: The following supporting information can be downloaded at https://www.mdpi.com/article/10.3390/agronomy16171747/s1. Table S1: China's official soil fertility classification criteria and the initial soil fertility in the 0–20 cm layer before sowing; Table S2: Yield and yield components during the 2022–2023 and 2023–2024 growing seasons; Table S3: Dry matter accumulation in different organs at maturity during the 2022–2023 and 2023–2024 wheat growing

seasons; Table S4: Pre-anthesis assimilate translocation from vegetative organs and post-anthesis assimilate accumulation to grain during the 2022–2023 and 2023–2024 wheat growing seasons; Table S5: Post-anthesis nitrogen remobilization and uptake during the 2022–2023 and 2023–2024 wheat growing seasons; Table S6: Nitrogen use efficiency and associated parameters during the 2022–2023 and 2023–2024 wheat growing seasons; Table S7: Root growth and morphological parameters at the booting stage during the 2023–2024 wheat growing seasons; Table S8: Nitrogen metabolism enzyme activities at the booting stage during the 2023–2024 wheat growing season; Table S9: Nitrogen metabolism enzyme activities at the grain filling stage during the 2023–2024 wheat growing season.

Author Contributions: Conceptualization, X.L., J.H., and R.L.; formal analysis, S.Z. and H.W.; investigation, S.Z. and X.G.; data curation, D.L.; writing—original draft preparation, X.L. and Q.F.; writing—review and editing, Q.F., J.H., D.L., and R.L.; visualization, X.G. and D.L.; supervision, H.W. and D.L.; project administration, R.L.; funding acquisition, R.L. and X.L. All authors have read and agreed to the published version of the manuscript.

Funding: This study was supported by the National Key Research and Development Program of China (2023YFD2301500).

Institutional Review Board Statement: Not applicable.

Informed Consent Statement: Not applicable.

Data Availability Statement: The data presented in this study are available on request from the corresponding author.

Conflicts of Interest: The authors declare no conflicts of interest.

References

1. Gao, Y.; Liu, Q. A new target for improving wheat end-use quality. *New Phytol.* **2023**, *239*, 5–6. [CrossRef]
2. Li, J.; Wang, Z.; Yao, C.; Zhang, Z.; Liu, Y.; Zhang, Y. Micro-sprinkling irrigation simultaneously improves grain yield and protein concentration of winter wheat in the North China Plain. *Crop. J.* **2021**, *9*, 1397–1407. [CrossRef]
3. Cui, Z.; Zhang, H.; Chen, X.; Zhang, C.; Ma, W.; Huang, C.; Zhang, W.; Mi, G.; Miao, Y.; Li, X.; et al. Pursuing sustainable productivity with millions of smallholder farmers. *Nature* **2018**, *555*, 363–366. [CrossRef]
4. Li, H.; Wang, H.; Fang, Q.; Jia, B.; Li, D.; He, J.; Li, R. Effects of irrigation and nitrogen application on NO_3^--N distribution in soil, nitrogen absorption, utilization and translocation by winter wheat. *Agric. Water Manag.* **2022**, *276*, 108058. [CrossRef]
5. Liu, C.; Wei, S.; Li, M.; Zhu, Q.; Cai, Y.; Han, G.; Lv, H.; Wang, Z.; Huang, D.; Wei, X.; et al. Nitrogen reduction via cultivation of green manures in drylands: A microbial perspective on enhancing soil nitrogen availability to increase wheat yield. *Agric. Ecosyst. Environ.* **2026**, *400*, 110208. [CrossRef]
6. Huang, C.; Chen, H.; Liu, X.; Ma, S.; Li, Y.; Zhang, Z.; Tang, H.; Wang, X.; Liu, Z. Effects of biochar on soil N_2O emissions, aggregate stability and nutrients under subsoiling and rotary tillage in wheat-maize rotation systems. *J. Agric. Food Res.* **2025**, *23*, 102208. [CrossRef]
7. Miressa, S.B.; Ding, Q.; Li, Y.; Amisi, E.O. Optimization of Tillage Operation Parameters to Enhance Straw Incorporation in Rice-Wheat Rotation Field. *Agriculture* **2025**, *15*, 54. [CrossRef]
8. Frayssinet, C.; Osterrieth, L.M.; Borrelli, L.N.; Honaine, M.F.; Ciarlo, E.; Heiland, P. Effect of silicate fertilizers on wheat and soil properties in Southeastern Buenos Aires province, Argentina. A preliminary study. *Soil Tillage Res.* **2019**, *195*, 104412. [CrossRef]
9. De Santis, M.A.; Ciavarella, F.; Pecorella, I.; Manganiello, C.; Flagella, Z.; Rinaldi, M. Climatic influence on yield stability in durum wheat genotypes grown under minimum tillage and no tillage management. *Field Crop. Res.* **2026**, *345*, 110561. [CrossRef]
10. Lyu, X.; Liu, Y.; Li, N.; Ku, L.; Hou, Y.; Wen, X. Foliar applications of various nitrogen (N) forms to winter wheat affect grain protein accumulation and quality via N metabolism and remobilization. *Crop. J.* **2022**, *10*, 1165–1177. [CrossRef]
11. Li, G.; Ren, X.; Pang, S.; Feng, C.; Niu, Y.; Qu, Y.; Liu, C.; Lin, X.; Wang, D. Nitrogen redistribution during the grain-filling stage and its correlation with senescence and *TaATG8* expression in leaves of winter wheat. *J. Integr. Agric.* **2026**, *25*, 1433–1442. [CrossRef]
12. Shi, X.; Liu, X.; Jing, J.; Zhang, Y.; Li, P.; Zong, Y.; Zhang, D.; Hao, X. Long-term no tillage straw mulching increased soil water and nitrogen storage in dryland wheat on the Loess Plateau, but may increase dissolved organic nitrogen leaching. *Field Crop. Res.* **2024**, *322*, 109705. [CrossRef]
13. Li, J.; Chen, L.; Zhang, C.; Ma, D.; Zhou, G.; Ning, Q.; Zhang, J. Combining rotary and deep tillage increases crop yields by improving the soil physical structure and accumulating organic carbon of subsoil. *Soil Tillage Res.* **2024**, *244*, 106252. [CrossRef]

14. Wang, W.; Yuan, P.; Shen, P.; Li, Y.; Hao, C.; Liao, Y.; Wen, X. Conservation tillage alters microbial nutrient limitations and carbon utilization efficiency by regulating microbial C-N-P metabolic function. *Agric. Ecosyst. Environ.* **2026**, *402*, 110328. [CrossRef]
15. Adil, M.; Wang, Z.; Chen, Y.; Lu, H.; Lu, S.; Bashir, S.; Gul, I.; Li, H.; Han, Z.; Feng, W. Long-term impacts of agronomic practices on winter wheat yield, water use efficiency, and nitrogen use efficiency in global dryland regions: A meta-analysis. *Soil Tillage Res.* **2025**, *253*, 106653. [CrossRef]
16. Wang, S.; Wang, H.; Hafeez, M.B.; Zhang, Q.; Yu, Q.; Wang, R.; Wang, X.; Li, J. No-tillage and subsoiling increased maize yields and soil water storage under varied rainfall distribution: A 9-year site-specific study in a semi-arid environment. *Field Crop. Res.* **2020**, *255*, 107867. [CrossRef]
17. Liang, Y.F.; Khan, S.; Ren, A.-X.; Lin, W.; Anwar, S.; Sun, M.; Gao, Z.-Q. Subsoiling and Sowing Time Influence Soil Water Content, Nitrogen Translocation and Yield of Dryland Winter Wheat. *Agronomy* **2019**, *9*, 37. [CrossRef]
18. Lv, Y.; Wang, S.; Xu, X.; Zhang, Y.; Shao, J.; Liu, X.; Li, R.; Gao, Q.; Bizimana, F.; Han, H.; et al. Optimizing subsoiling depth to enhance soil water storage and annual crop water productivity in wheat-maize cropping system. *Agric. Water Manag.* **2026**, *325*, 110199. [CrossRef]
19. Wang, H.; Zhang, D.; He, J.; Wang, L.; Ren, J.; Zhang, S.; Bai, W.; Song, J.; Lv, G.; Li, J. Changes in Soil Properties, Bacterial Communities and Wheat Roots Responding to Subsoiling in South Loess Plateau of China. *Agronomy* **2022**, *12*, 2288. [CrossRef]
20. Li, M.; Zhang, L.; Li, Y.; Cao, Y.; Zhang, Y.; Gao, Z.; Zhang, D.; Lin, W. Root–Canopy Coordination Drives High Yield and Nitrogen Use Efficiency in Dryland Winter Wheat. *Plants* **2026**, *15*, 153. [CrossRef]
21. Li, P.; Ma, B.; Palta, J.A.; Wei, X.; Guo, S.; Ding, T.; Ma, Y. Distinctive root system adaptation of ploidy wheats to water stress: A cue to yield enhancement. *J. Agron. Crop. Sci.* **2023**, *209*, 566–577. [CrossRef]
22. Li, X.; Wang, R.; Lou, F.; Ji, P.; Wang, J.; Dong, W.; Tao, P.; Zhang, Y. Subsoiling combine with layered nitrogen application optimizes root distribution and improve grain yield and N efficiency of summer maize. *Agronomy* **2024**, *14*, 1228. [CrossRef]
23. Odone, A.; Popovic, O.; Thorup-Kristensen, K. Deep roots: Implications for nitrogen uptake and drought tolerance among winter wheat cultivars. *Plant Soil* **2024**, *500*, 13–32. [CrossRef]
24. Fernando, E.A.J.; Selvaraj, M.; Uga, Y.; Busch, W.; Bowers, H.; Tohme, J. Going deep: Roots, carbon, and analyzing subsoil carbon dynamics. *Mol. Plant* **2024**, *17*, 1–3. [CrossRef]
25. Wang, R.; Dijkstra, F.A.; Han, X.; Jiang, Y. Root nitrogen reallocation: What makes it matter? *Trends Plant Sci.* **2024**, *29*, 1077–1088. [CrossRef]
26. Zhao, L.; Li, L.; Song, L.; Liu, Z.; Li, X.; Li, X. HMW-GS at *Glu-B1* Locus Affects Gluten Quality Possibly Regulated by the Expression of Nitrogen Metabolism Enzymes and Glutenin-Related Genes in Wheat. *J. Agric. Food Chem.* **2020**, *68*, 5426–5436. [CrossRef]
27. Hirel, B.; Le Gouis, J.; Ney, B.; Gallais, A. The challenge of improving nitrogen use efficiency in crop plants: Towards a more central role for genetic variability and quantitative genetics within integrated approaches. *J. Exp. Bot.* **2007**, *58*, 2369–2387. [CrossRef]
28. Wang, J.; Wang, Z.; Gu, F.; Liu, H.; Kang, G.; Feng, W.; Wang, Y.; Guo, T. Tillage and irrigation increase wheat root systems at deep soil layer and grain yields in lime concretion black soil. *Sci. Rep.* **2021**, *11*, 6394. [CrossRef]
29. Dasgupta, D.; Camuy-Vélez, L.A.; Nath, D.; Zitnick-Anderson, K.; Aberle, E.; Banerjee, S. Fertilizer level has a stronger effect than tillage intensity on crop microbiome recruitment. *Agric. Ecosyst. Environ.* **2026**, *399*, 110144. [CrossRef]
30. Zhu, Y.; Liu, J.; Li, J.; Xian, L.; Chu, J.; Liu, H.; Song, J.; Sun, Y.; Dai, Z. Delayed sowing increased dry matter accumulation during stem elongation in winter wheat by improving photosynthetic yield and nitrogen accumulation. *Eur. J. Agron.* **2023**, *151*, 127004. [CrossRef]
31. Liao, Z.; Zeng, H.; Fan, J.; Lai, Z.; Zhang, C.; Zhang, F.; Wang, H.; Cheng, M.; Guo, J.; Li, Z.; et al. Effects of plant density, nitrogen rate and supplemental irrigation on photosynthesis, root growth, seed yield and water-nitrogen use efficiency of soybean under ridge-furrow plastic mulching. *Agric. Water Manag.* **2022**, *268*, 107688. [CrossRef]
32. Tian, Z.; Yin, Y.; Li, B.; Zhong, K.; Liu, X.; Jiang, D.; Cao, W.; Dai, T. Optimizing planting density and nitrogen application to mitigate yield loss and improve grain quality of late-sown wheat under rice–wheat rotation. *J. Integr. Agric.* **2025**, *24*, 2558–2574. [CrossRef]
33. Colombi, T.; Keller, T. Developing strategies to recover crop productivity after soil compaction—A plant eco-physiological perspective. *Soil Tillage Res.* **2019**, *191*, 156–161. [CrossRef]
34. Reynolds, M.; Foulkes, J.; Furbank, R.; Griffiths, S.; King, J.; Murchie, E.; Parry, M.; Slafer, G. Achieving yield gains in wheat. *Plant Cell Environ.* **2012**, *35*, 1799–1823. [CrossRef]
35. Lynch, J.P. Harnessing root architecture to address global challenges. *Plant J.* **2021**, *109*, 415–431. [CrossRef]
36. Thorup-Kristensen, K.; Halberg, N.; Nicolaisen, M.; Olesen, J.E.; Crews, T.E.; Hinsinger, P.; Kirkegaard, J.; Pierret, A.; Dresbøll, D.B. Digging Deeper for Agricultural Resources, the Value of Deep Rooting. *Trends Plant Sci.* **2020**, *25*, 406–417. [CrossRef]
37. Haymaker, J.R.; Stewart, R.D.; Wolters, B.; Stephenson, K.; Balkcom, K.S.; Reiter, M.S. Long-term effects of cover crops and no-tillage on soil health in the Virginia Coastal Plain. *Soil Tillage Res.* **2026**, *256*, 106898. [CrossRef]

38. Hawkesford, M.J.; Riche, A.B. Impacts of G × E × M on nitrogen use efficiency in wheat and future prospects. *Front. Plant Sci.* **2020**, *11*, 1157. [CrossRef]
39. Tegeder, M.; Masclaux-Daubresse, C. Source and sink mechanisms of nitrogen transport and use. *New Phytol.* **2018**, *217*, 35–53. [CrossRef]
40. Cassman, K.G.; Dobermann, A. Nitrogen and the future of agriculture: 20 years on. *Ambio* **2022**, *51*, 17–24. [CrossRef]
41. Sun, C.-H.; Yu, J.-Q.; Hu, D.-G. Nitrate: A crucial signal during lateral roots development. *Front. Plant Sci.* **2017**, *8*, 485. [CrossRef]
42. Liu, K.-H.; Liu, M.; Lin, Z.; Wang, Z.-F.; Chen, B.; Liu, C.; Guo, A.; Konishi, M.; Yanagisawa, S.; Wagner, G.; et al. NIN-like protein 7 transcription factor is a plant nitrate sensor. *Science* **2022**, *377*, 1419–1425. [CrossRef]
43. Xu, G.; Fan, X.; Miller, A.J. Plant nitrogen assimilation and use efficiency. *Annu. Rev. Plant Biol.* **2012**, *63*, 153–182. [CrossRef]
44. Wen, B.; Li, C.; Fu, X.; Li, D.; Li, L.; Chen, X.; Wu, H.; Cui, X.; Zhang, X.; Shen, H.; et al. Effects of nitrate deficiency on nitrate assimilation and chlorophyll synthesis of detached apple leaves. *Plant Physiol. Biochem.* **2019**, *142*, 363–371. [CrossRef]